

pubs.acs.org/JPCA Article

Halide Size-Selective Binding by Cucurbit[5]uril—Alkali Cation Complexes in the Gas Phase

Tina Heravi,[†] Jiewen Shen,[†] Spencer Johnson, Matthew C. Asplund, and David V. Dearden*



Cite This: J. Phys. Chem. A 2021, 125, 7803–7812



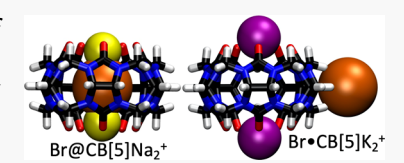
ACCESS

Metrics & More



Supporting Information

ABSTRACT: We report data that suggest complexes with alkali cations capping the portals of cucurbit[5]uril (CB[5]) bind halide anions size-selectively as observed in the gas phase: Cl⁻ binds inside the CB[5] cavity, Br⁻ is observed both inside and outside, and I⁻ binds weakly outside. This is reflected in sustained off-resonance irradiation collision-induced dissociation (SORI-CID) experiments: all detected Cl⁻ complexes dissociate at higher energies, and Br⁻ complexes exhibit unusual bimodal dissociation behavior, with part of the ion population



dissociating at very low energies and the remainder dissociating at significantly higher energies comparable to those observed for Cl⁻. Decoherence cross sections measured in SF₆ using cross-sectional areas by Fourier transform ion cyclotron resonance techniques for $[CB[5] + M_2X]^+$ (M = Na, X = Cl or Br) are comparable to or less than that of $[CB[5] + Na]^+$ over a wide energy range, suggesting that Cl⁻ or Br⁻ in these complexes are bound inside the CB[5] cavity. In contrast, $[CB[5] + K_2Br]^+$ has a cross section measured about 20% larger than that of $[CB[5] + Na]^+$, suggesting external binding that may correspond with the weakly bound component seen in SORI. While I⁻ complexes with alkali cation caps were not observed, alkaline earth iodides with CB[5] yielded complexes with cross sections 5–10% larger than that of $[CB[5] + Na]^+$, suggesting externally bound iodide. Geometry optimization at the M06-2X/6-31+G* level of *ab initio* theory suggests that internal anion binding is energetically favored by approximately 50–200 kJ mol⁻¹ over external binding; thus, the externally bound complexes observed experimentally must be due to large energetic barriers hindering the passing of large anions through the CB[5] portal, preventing access to the interior. Calculation of the barriers to anion egress using MMFF//M06-2X/6-31+G* theory supports this idea and suggests that the size-selective binding we observe is due to anion size-dependent differences in the barriers.

■ INTRODUCTION

Many strategies for selective binding of anions are targeted at polyatomic anions and their hydrogen-bonding preferences. Therefore, these strategies tend to be shape-selective for particular anions. While the selective binding of cations based on complementarity between the sizes of the guest and host is relatively common, similar size-based selectivity for anions is relatively rare, although it is not unknown.²

Binding of the spherical halide anions depends strongly on the extent to which the anion is solvated; so, for example, complexation of fluoride in protic solvents is very difficult because few hosts can compete effectively against fluoride's very high solvation energy. The larger halides have progressively lower solvation energies, but their larger sizes also mean that electrostatic interactions with potential hosts are weaker. Chloride seems to offer a good compromise between these opposing considerations, with many examples of chloride-binding and transporting systems known, 1,3,4 although usually selectivity for one halide over another is not addressed.

Cucurbit[n]urils (hereafter CB[n], where n indicates the number of repeat units), which are cyclic condensation polymers of glycoluril and formaldehyde (Figure 1), are fairly rigid host molecules. Both the roughly spherical electropositive interior of the hollow CB[n]—metal ion complex, and to a lesser extent the roughly circular portal that grants access to the interior, have relatively well-defined sizes that can lead to

size-selective binding of spherical halide anions. Such size selectivity has frequently been observed for both neutral and cationic guests in CB[n] hosts. ⁵⁻⁷ As the potential maps in Figure 1b,c suggest, CB[5] itself is probably not a good host for anions. However, the two portals of CB[5] (at the top and bottom of the ligand as oriented in the figure) are excellent cation-binding sites, and complexes of CB[5] with cations have electrostatic potentials that suggest anion binding in the host cavity should be favorable (Figure 1c). As a simple, rigid, ditopic host with two well-defined cation-binding sites, CB[5] offers an opportunity to examine how two proximate cation-binding sites interact and how that interaction can be modulated in the presence of an anion.

A few reports^{8–10} have examined CB[n]-based systems as anion receptors but to our knowledge have not addressed anion size selectivity. For example, Huang and co-workers synthesized chloride and nitrate anion inclusion complexes of CB[5]—metal species and explored selectivity and metal ion

Received: June 8, 2021
Published: September 7, 2021



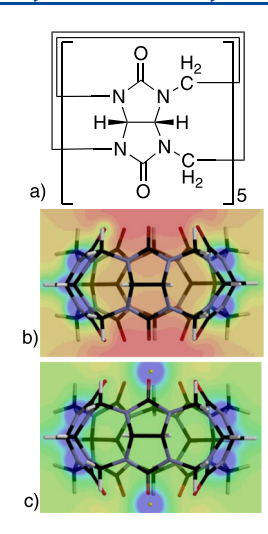


Figure 1. (a) Structure of cucurbit[5]uril (CB[5]). (b) Electrostatic potential contours on a plane through CB[5] (red = negative, blue = positive). (c) Electrostatic potential contours on a plane through $[CB[5] + Na_2]^{2+}$, with the same color coding over the same range of values.

effects using X-ray crystallography and fluorescence spectroscopy. ^{8,9} In particular, they synthesized Cl@CB[5] inclusion complexes capped by various metals (K⁺, Ba²⁺, Cd²⁺, and La³⁺) and examined binding behaviors. For K⁺ and Ba²⁺ cations, anion complexes of CB[5] bound one metal ion on each portal, while for Cd²⁺ or La³⁺, only one metal ion was bound on one of the portals (leaving the other portal open). With K⁺, a one-dimensional polycationic chain formed, whereas the other three cations resulted in isolated complexes. This condensed phase work also examined the selectivity of CB[5] toward nitrate and chloride and found that protonated CB[5] favored binding nitrate, whereas coordination of La(III) to CB[5] resulted in a preference for chloride over nitrate in solution and in the solid state.

More recent studies have explored molecules that share structural similarity with cucurbiturils as halide binders, including bambusurils ^{11–13} and hemicucurbit[6]urils. ¹⁴ With these hosts, binding involves interactions of H atoms on the host with the halide. This contrasts with the present work, where we will show that preferential binding occurs inside the CB[5]—metal complex cavity where there are no proximate H atoms; instead, halide binding in CB[5] is largely governed by electrostatic considerations and is strongly dependent on the size relationship between the structural features of the host and the halide anion.

Herein, we extend the study of halide binding by CB[5] capped with various metal ions into the gas phase and, in particular, demonstrate size selectivity and some degree of metal dependence in these interactions. Our goals included understanding size-based anion-binding selectivity in the absence of solvent effects, combining experimental and computational approaches to probe the intrinsic binding properties of these host—guest systems without the influence of neighboring molecules, and developing the ability to perform these studies with very small amounts of material, in complex mixtures, without requiring crystals. We employed a combination of gas-phase experimental and computational methods toward these objectives. We measured relative dissociation energies of various complexes involving halide anions, CB[5], and metal cations using the sustained off-

resonance irradiation collision-induced dissociation (SORI-CID) technique ^{15,16} and measured relative collision cross sections (CCS)—which yield gas-phase geometric information otherwise difficult to obtain—using a new variant (unpublished results, which we refer to as "multi-CRAFTI") of the cross-sectional areas by Fourier transform ion cyclotron resonance (CRAFTI) technique. ^{17–20} We complemented the experimental results with computed binding energies using the M06-2X/6-31+G* level of density functional theory and also calculated the barriers to anion egress using the structures determined from the Merck molecular force field (MMFF), with energies calculated using M06-2X/6-31+G* theory. Taken together, we believe that the results make a strong case for size-selective binding of halide anions by CB[5], based on the relative sizes of the halides and the CB[5] portals.

EXPERIMENTAL SECTION

Materials. CB[5], as well as fluorides, bromides, and iodides of sodium and potassium, and rubidium chloride (all with ≥99% purity) were purchased from Sigma-Aldrich (St. Louis, MO). Sodium chloride was analytical reagent grade from Mallinckrodt Chemical Works (St. Louis, MO); potassium chloride was reagent grade from Merck & Co. (Kenilworth, NJ). Barium iodide (≥95% purity) and strontium iodide (≥99% purity) were purchased from Aldrich (Milwaukee, WI). HPLC-grade water from Avantor Performance Materials (Center Valley, PA) and isopropyl alcohol (≥99.5% purity) from Thermo Fisher Scientific (Fair Lawn, NJ) were used for all solutions. Argon (Ar) and sulfur hexafluoride (SF₆) gases (99.9997 and 99.8% purity, respectively) were purchased from Airgas, Inc. (Radnor, PA). Solvents, CB[5], and the metal salts were used as supplied without further purification.

Stock solutions of CB[5] and metal salts were prepared at about 4 mM concentration in 50:50 isopropanol/water. Solutions for electrospray were prepared by mixing and diluting the stock solutions with 50:50 isopropanol/water so that the final concentration of CB[5] was 100 μ M and the alkali metal halide concentration was about 200 μ M.

Instrumentation. All experiments were performed using a Bruker model APEX 47e Fourier transform ion cyclotron resonance mass spectrometer (FTICR-MS), equipped with an Infinity trapping cell²¹ and a 4.7 T superconducting magnet, and controlled by a MIDAS Predator data system (National High Magnetic Field Ion Cyclotron Resonance Facility, Tallahassee, FL).²² Collision gas (Ar for SORI experiments and SF₆ for CRAFTI) was introduced to the FTICR trapping cell using a Freiser-type²³ pulsed leak valve consisting of a 0.004" orifice solenoid pressurization valve backed by a 28 psig supply line and a 0.039" orifice solenoid evacuation valve connected to a mechanical vacuum pump (both valves from General Valve Corp., Fairfield, NJ). Both solenoid valves were connected to the high-pressure side of a precision variable leak valve (Varian, Palo Alto, CA). Pressure measurements were carried out using a cold cathode gauge (Balzers; Fürstentum, Lichtenstein) mounted outside the high magnetic field about 1 m from the trapping cell. Various steady-state backing pressures for the leak were obtained by varying the length of time the pressurization solenoid valve was left open, while the evacuation solenoid is left closed, resulting in a corresponding constant pressure in the trapping cell about 0.5 s after the pressurization event. Ions were generated in a micro-electrospray source modified from an Analytica (Branford, CT, USA)

design, with a heated metal capillary drying tube based on the design of Eyler. ²⁴ Radio frequency (rf) excitation amplitudes were measured using an oscilloscope at the output of the final excitation amplifier. The ions being compared in multi-CRAFTI experiments were excited using waveforms synthesized via a LabVIEW program. The program produces an excitation waveform with a user-specified duration by adding appropriate single-frequency excitation waveforms with relative amplitudes such that both the ions being compared are excited to the same center-of-mass kinetic energy. Thus, both ions were excited simultaneously at their respective cyclotron frequencies.

Procedures for SORI-CID and Multi-CRAFTI. In all experiments, ions were generated via electrospray and injected into the FTICR trapping cell. Mono-isotopic peaks were isolated using stored waveform inverse Fourier transform techniques²⁵ and then subjected to either SORI-CID or multi-CRAFTI.

In SORI-CID experiments,²⁶ the background Ar collision gas pressure in the trapping cell was raised to 10⁻⁵ mbar via the pulsed leak valve, waiting 3 s after pulsed leak activation to ensure steady-state pressure conditions, followed by a computer-controlled duration, single-frequency, fixed amplitude RF pulse 500 or 1000 Hz below the resonant frequency of the ion of interest. This was followed by evacuation of the pulsed leak for 3 s to allow the cell to return to the baseline pressure of around 10⁻⁸ mbar, immediately followed by a broad-band chirp excitation and detection. A tool command language (TCL) script was used to modulate the SORI-CID energy deposited into the target ions by varying the duration of the single-frequency SORI-CID excitation event.

The average energy deposited in the ion via the SORI-CID event, $E_{\rm SORI}$, is calculated using 27

$$E_{\text{SORI}} = N^* \sigma K_y f_E t_{\text{coll}} \frac{\beta^3 q^3}{128\pi^3 d^3 (\Delta f)^3} \left(\frac{M}{M+m}\right) \frac{V_{\text{pp}}^{\ 3}}{m^2}$$
 (1)

Here, N^* is the neutral gas number density, σ is the CCS, $K_{\rm v}$ is a proportionality constant, $f_{\rm E}$ is an assumed constant fraction of the maximum kinetic energy converted to internal energy in the ion, $t_{\rm coll}$ is the length of the SORI event, β is the trapping cell geometry factor (0.897 in the Bruker Infinity Cell used in these experiments), 21 q is the charge on the ion, d is the trapping cell diameter, Δf is the frequency offset of the excitation pulse from the ion's resonant frequency, M is the mass of the neutral, m is the mass of the ion, and $V_{\rm pp}$ is the peak-to-peak amplitude of the SORI excitation pulse.

In multi-CRAFTI experiments, collision gas was admitted into the trapping cell using the pulsed leak valve, followed by a 3 s delay to allow collisional damping of possible residual excitation from the isolation. The pressure in the trapping cell was controlled by varying the duration of the pulsed leak pressurization event using a TCL script. The ions were translationally excited via a dual-frequency RF pulse containing components at each of their resonant cyclotron frequencies for (typically) 350 μ s (with excitation times deliberately kept short to minimize collisions during the excitation), followed by the detection of the resulting transient signal at the constant, elevated pressure. Signal detection was always of sufficient duration that the signal damped back to background levels. SF₆ was used as the collision gas in these experiments because it enables higher center-of-mass kinetic energy at orbital velocities that allow the ion to remain inside the trapping

cell. The resulting time domain image current signal yields a frequency domain power spectrum after Fourier transformation with one zero fill and no apodization; typically, about 10–20 scans were averaged for each spectrum depending on the intensity of the signal.

Computational Modeling. Natural abundance isotope patterns for comparison with the experiment were computed using the Scientific Instrument Services Web site: https://www.sisweb.com/mstools/isotope.htm.

Molecular structures were obtained using the Spartan '18 package (Wavefunction, Inc., Irvine, CA, USA) for conformational searching with the Merck molecular force field (MMFF) provided in the package, requesting 10,000 starting conformers (but systematic searches sometimes completed after examining fewer than 10,000 structures). Geometry optimization calculations were performed using density functional theory (M06-2X/6-31+G*, employing the LANL2DZ basis set for atoms not described by the 6-31+G* basis), as implemented in the NWChem²⁸ computational package.

Barriers to anion egress were also calculated using Spartan '18. In these calculations, Spartan's "Energy Profile" mode was used with MMFF while constraining and systematically increasing the distance between two of the cucurbituril N atoms and the halide anion. Positions of the N atoms were frozen to keep the cucurbituril stationary, but the positions of all other atoms were allowed to fully relax at each step. This forces the anion to egress the CB[5] host without causing significant distortion of the host beyond what is required to allow the anion to leave the host cavity. The geometries obtained from the Energy Profile calculation were then used for single-point energy calculations at the M06-2X/6-31+G* level of theory. Energies relative to the energetic minimum with the anion in the center of the host cavity were then determined and related to the distance of the anion from the center of mass of the host.

Data Analysis. Transient signals were analyzed using the Igor Pro software package (versions 7 and 8 (64-bit); Wavemetrics, Lake Oswego, OR, USA). For SORI experiments, the Igor program was used to extract peak amplitudes for a set of spectra that differ in SORI excitation times, followed by the generation of tables of peak intensities as a function of SORI excitation duration. The resulting parent and product ion peak intensities were normalized against their sum, and the relative SORI collision energy was determined from the excitation time scaled to account for the differences in mass, pressure, and excitation amplitude (although most experiments were conducted while maintaining a constant excitation amplitude). Energies obtained from these SORI-CID experiments may be compared qualitatively but not quantitatively due to uncertainties about the absolute kinetic energies of the colliding partners, number of collisions required for dissociation, and conversion efficiency from kinetic to internal energy.

For multi-CRAFTI experiments, at each collision energy, a set of power spectra measured at various pressures of the collision gas was collected for each of the two ions being compared. Experimental results were processed using the Igor

Pro software package. The CCS ratio of the two ions $\left(\frac{\sigma_1}{\sigma_2}\right)$ was determined from the linewidths of the ions using eq 2^{17}

$$\frac{\sigma_{1}}{\sigma_{2}} = \frac{\text{fwhm}_{1}}{\text{fwhm}_{2}} \frac{m_{1}z_{2}}{m_{2}z_{1}} \frac{V_{\text{PP},2}t_{\text{exc},2}}{V_{\text{PP},1}t_{\text{exc},1}}$$
(2)

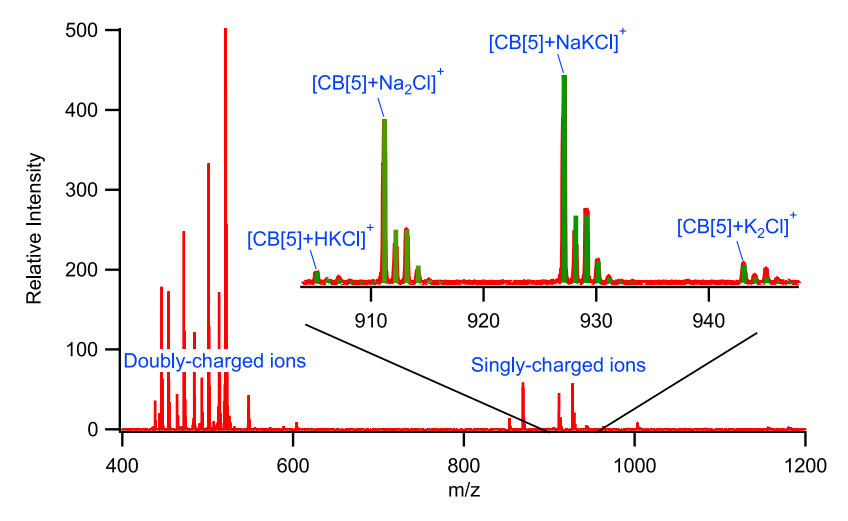


Figure 2. Electrospray mass spectrum for CB[5] mixed with NaCl and KCl. Inset: expansion from m/z 900 to 950. Computed isotopic patterns are overlaid in green.

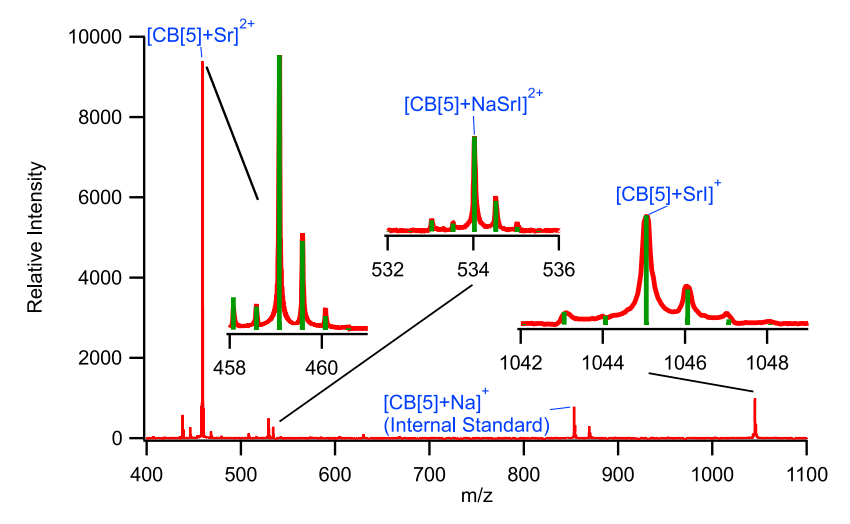


Figure 3. Electrospray mass spectrum for CB[5] mixed with SrI_2 . Insets: expansions showing isotopic patterns resulting from complexation, with computed isotopic distributions overlaid in green.

Here, $fwhm_n$ is the full width at half-maximum linewidth obtained from Lorentzian fits of the power spectral line for each ion, and z_n is the ion charge. The excitation durations for the two ions, $t_{exc,n}$ are the same, so that the $t_{exc,n}$ terms cancel. All other parameters are the same as defined above.

RESULTS

Electrospray of CB[5] with Alkali Metal Salts. When solutions containing CB[5] and sodium or potassium halide salts were electrosprayed (Figures 2 and S1), significant relative abundances were observed for complexes containing either the Cl $^-$ or Br $^-$ ion, but no F $^-$ or I $^-$ complexes were observed. In the mass spectra, exact masses agree with the computed masses within 15 ppm or better, and experimental isotopic patterns are in reasonable agreement with the computed patterns. The observed complexes had general stoichiometry [CB[5] + M₂X] $^+$, where M = Na or K and X = Cl or Br.

The intensities of the halide-containing ions were strongly dependent on the conditions in the electrospray ion source and tended to be stronger under conditions where the collision energies in the source were minimized. Although the relative

abundances of the halide-containing peaks were often small, this does not imply that these peaks are unimportant. In all cases, the signal-to-noise was sufficient to allow clear identification. Relative abundances of peaks in the electrospray mass spectra do not necessarily reflect the relative abundances of the corresponding species in solution, often being strongly affected by ion source conditions, electrospray efficiency, surface activity, solvation energies, and so forth. 29–32

Attempts to electrospray fluoride or iodide salts of alkali metals resulted in intense signals for $[CB[5] + M]^+$ without any detected fluoride or iodide complexes. When electrospraying solutions containing CB[5] and alkaline earth halides, signals for $[CB[5] + SrI]^+$, $[CB[5] + BaI]^+$, and $[CB[5] + NaBaI]^{2+}$ were observed. The spectra are shown in Figures 3 and S2.

Sustained Off-Resonance Irradiation Collision-Induced Dissociation. Energy-resolved SORI experiments are designed to show how ions fragment as a function of relative kinetic energy, $E_{\rm SORI}$. We performed SORI for the dissociation of chloride and bromide complexes, $[{\rm CB[5]} + {\rm M_2X}]^+$ (M = Na or K; X = Cl or Br)—see Figure 4. Each of the points is an average from at least three separate measurements, and the error bars represent standard deviations. Dissociation occurred

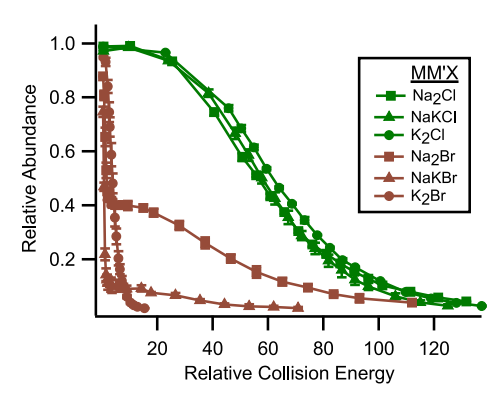


Figure 4. Parent ion survival curves for $[CB[5] + MM'X]^+$ obtained by SORI-CID techniques. Points are averages of three or more runs, error bars are standard deviations, and lines are fits of one or two sigmoids to the data.

exclusively by the loss of MX. All the chloride-containing complexes exhibit dissociation that is easily fit to a single sigmoid and have similar, relatively high dissociation energies. In contrast, the bromide-containing $[CB[5] + NaKBr]^+$ and $[CB[5] + Na_2Br]^+$ complexes exhibit interesting bimodal dissociation behavior, fit using two sigmoids, in which some of the ions fragment at very low relative collision energies but the remainder require much higher relative energies, similar to those required to dissociate $[CB[5] + M_2Cl]^+$. The higher energy dissociation pathway was not observed for $[CB[5] + K_2Br]^+$, which dissociates at much lower energy than the chloride-containing complexes and at similar energies to those observed for the low-energy portion of the dissociation of $[CB[5] + NaKBr]^+$ and $[CB[5] + Na_2Br]^+$.

We examined the dissociation of the mixed metal complexes more closely as two dissociation channels are possible in these systems. For example, the [CB[5] + NaKCl]⁺ complex dissociates either by the loss of NaCl or by the loss of KCl. As Figure 5 shows, the loss of NaCl is more facile at higher

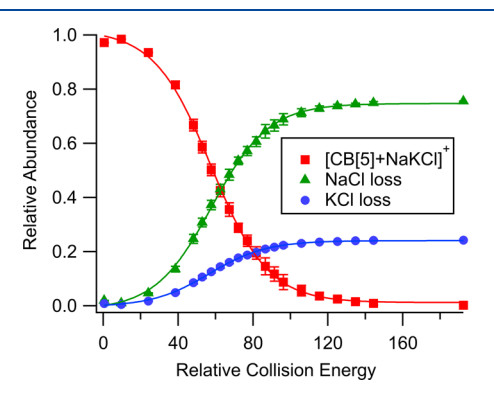


Figure 5. Relative $E_{\rm SORI}$ for the dissociation of $[{\rm CB[5]} + {\rm NaKCl}]^+$. Points are averages of three or more runs, error bars are standard deviations, and lines are sigmoidal fits to the data.

energies, about 3 times more prevalent than the loss of KCl. A similar result was found when dissociating chloride complexes with one K⁺ and one Rb⁺ (Figure S3). Again, the system has two dissociation products, and dissociation by the loss of RbCl is slightly favored over the loss of KCl. Similarly, both channels were observed in the dissociation of [CB[5] + NaKBr]⁺, with about 75% dissociating via the loss of NaBr and 25% via the loss of KBr (see Figure 6). As was noted above (Figure 4), the

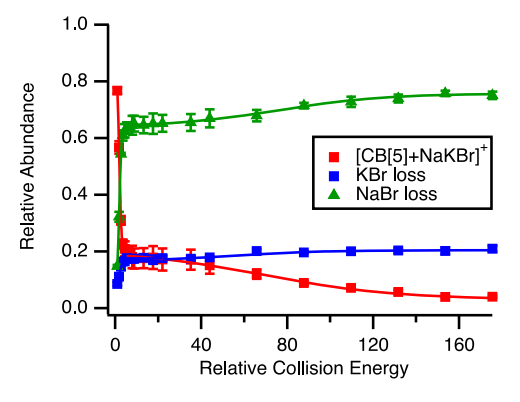


Figure 6. Relative $E_{\rm SORI}$ for the dissociation of $[{\rm CB}[5] + {\rm NaKBr}]^+$. Points are averages of five runs, error bars are standard deviations, and lines are sigmoidal fits to the data (two sigmoids for each set).

loss of the parent ion appears to be bimodal, as does the appearance of both product ions, which are produced primarily at low total SORI energies with a smaller contribution at significantly higher energies.

Multi-CRAFTI Experiments. Our attempts to measure CCS using more conventional ion mobility techniques for the halide-containing complexes were unsuccessful, probably due to the relative fragility of these complexes in the gas phase and the fact that mobility measurements require multiple low-energy ion-neutral collisions that potentially result in the dissociation of these fragile ions. CRAFTI techniques, where ions are kept under ultrahigh vacuum conditions for most of the experiment, enabled the measurement of relative CCS for more fragile species.

CRAFTI cross sections of supramolecules increase with increasing center-of-mass kinetic energy until they reach a limiting value that is generally similar to the hard-sphere cross section computed from the expected molecular structure. ¹⁸ In the current study, "multi-CRAFTI" experiments were performed for the target ions and internal standards for each system simultaneously over a range of kinetic energies obtained by adjusting the amplitudes of the rf excitation waveforms. We have observed that relative cross sections approach limiting values at lower energies than do absolute cross sections (unpublished results).

The results of multi-CRAFTI experiments for CB[5]—alkali halide complexes are shown in Figure 7. Except for the lowest energy point (near 20 eV) in Figure 7 (where we might expect multicollision dephasing to confound the results), 17,18 the measured ($^{\text{CRAFTI}}\text{CCS}_{\text{SF6}}([\text{CB[5]} + \text{M}_2\text{X}]^+))/(^{\text{CRAFTI}}\text{CCS}_{\text{SF6}}([\text{CB[5]} + \text{Na}]^+))$ ratios remain fairly constant as a function of energy. At higher energies, all the ratios average around 1 or less except in the case of $[\text{CB[5]} + \text{K}_2\text{Br}]^+$, which has a ratio of about 1.2.

Relative CCS were measured for the iodide-containing ions using the same internal standard, $[CB[5] + Na]^+$. $(^{CRAFTI}CCS_{SF6}([CB[5] + AI]^+))/(^{CRAFTI}CCS_{SF6}([CB[5] + Na]^+))$ (where A=Sr or Ba) ratios are shown in Figure 8. The iodide-containing ions have cross sections about 5% larger than that of CB[5] binding a single Na^+ , suggesting that iodide is attached to the exterior of the complex, outside the cavity. Given the large size of I^- (ionic radius 206 pm) 33 relative to the CB[5] portal (radius 120 pm) and cavity (radius 220 pm), 34 this is not surprising. The $[CB[5] + SrI]^+$ and $[CB[5] + BaI]^+$ ions have cross sections that are approximately the same within the experimental error.

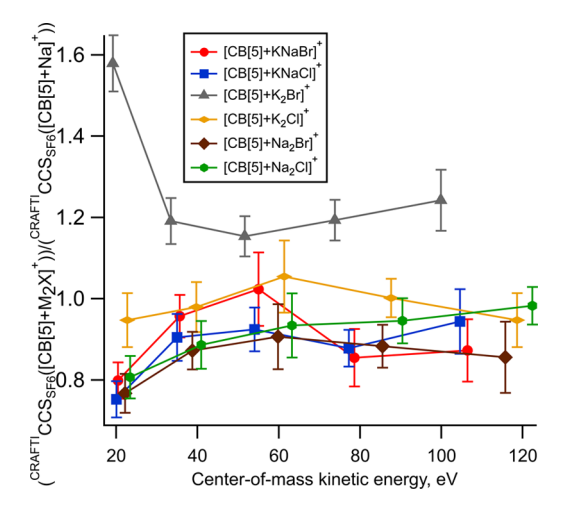


Figure 7. Multi-CRAFTI CCS in SF₆ for $[CB[5] + M_2X]^+$ (M = Na, K; X = Cl, Br) relative to that of $[CB[5] + Na]^+$. Points are averages of three or more runs, error bars are standard errors, and lines are simply to guide the eye.

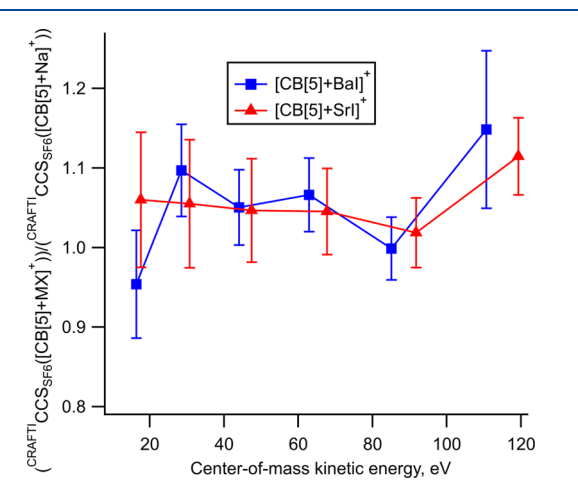


Figure 8. Multi-CRAFTI CCS in SF_6 for $[CB[5] + SrI]^+$ and $[CB[5] + BaI]^+$ relative to that of $[CB[5] + Na]^+$. Points are averages of three or more runs, error bars are standard errors, and lines are simply to guide the eye.

For $[CB[5] + NaBaI]^{2+}$, we were unable to simultaneously observe $[CB[5] + Na]^+$ and $[CB[5] + NaBaI]^{2+}$, so we used a different internal standard, the easily observed $[CB[5] + Ba]^{2+}$ ion. The result is shown in Figure S4. All the measured ratios are significantly greater than 1, which suggests that $[CB[5] + NaBaI]^{2+}$ is significantly larger than $[CB[5] + Ba]^{2+}$.

Computational Results. Modeling suggests at least eight distinct binding motifs for the [CB[5] + NaKBr]+ complex, illustrated in Figure 9, which are qualitatively similar to the binding motifs found for the other halide anions. Of these, that in Figure 9a, with Br bound internally, is by far the lowest in energy according to M06-2X/6-31+G* modeling. All the remaining seven structures have bromide externally bound. The lowest energy external structure, Figure 9b, places Br on the CB[5] equator, centered over an eight-membered ring composed of 4 C and 4 N atoms, but is calculated to be 181 kJ mol⁻¹ higher in energy than the structure with Br bound internally. Placement of Br over a five-membered ring of CB[5] results in higher energies, up 15 or 16 kJ mol⁻¹ higher than the equatorial structure, depending on whether the fivemembered ring is closer to the Na+- or K+-bound portal of CB[5], respectively. Placement of Br externally but closer to the CB[5] axis results in higher energies; in Figure 9e, with a 118° K-Na-Br angle, it is 44 kJ mol⁻¹ higher than the equatorial placement, and in Figure 9f, with a 171° K-Na-Br angle, it is 81 kJ mol⁻¹ higher than the equatorial structure. Placement of both metal ions and the bromide ion on the same CB[5] portal, Figure 9g,h, was only slightly higher than the 171° structure.

Table 1 compiles the computed energies at 0 K for the process $[CB[5] + M]^+ + MX \rightarrow [CB[5] + M_2X]^+$ (binding of MX to $[CB[5] + M]^+$), using the lowest energy anion structures bound internally and externally. For X = Cl, Br, or I, the internally bound complexes have energies 160-215 kJ mol⁻¹ lower than the corresponding externally bound complexes, whereas for X = F, the internally bound complexes are still favored but by a smaller amount.

Comparing the halides, the computed order of binding for the internal complexes is $Br^- > I^- > Cl^- > F^-$ with sodium, while with potassium the order is $I^- > Br^- > Cl^- > F^-$. For externally bound complexes, the binding energy of each of the halides is similar, spanning a range of 19 kJ mol⁻¹ for the Na-

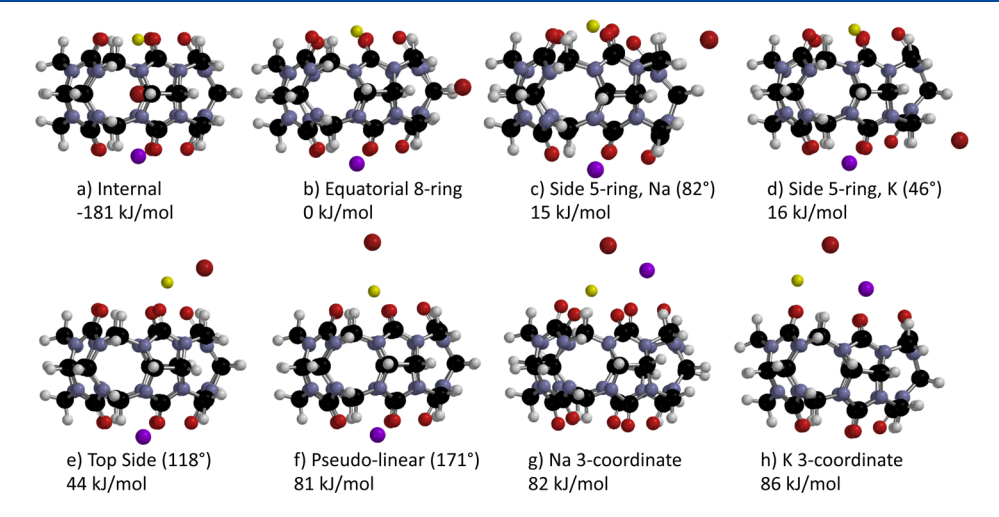


Figure 9. M06-2X/6-31+G*-computed structures and relative energies for [CB[5] + NaKBr]⁺. H atoms are white, C are black, N are blue, O are red, Na are yellow, K are purple, and Br are dark red. Angles in parentheses are K-Na-Br angles.

Table 1. Energies for $[CB[5] + M]^+ + MX \rightarrow [CB[5] + M_2X]^+$ Computed at the M06-2X/6-31+G* Level of Theory

		energy for $[CB[5] + M]^+ + MX \rightarrow [CB[5] + M_2X]^+$ (kJ mol ⁻¹)					
		M = Na			M = K		
anion, X	ionic radius ³⁵ (pm)	internal	external	internal — external	internal	external	internal – external
F	119	-306	-212	-94	-311	-257	-54
Cl	167	-399	-193	-206	-392	-229	-163
Br	182	-425	-212	-213	-433	-256	-177
I	206	-417	-202	-215	-436	-245	-190

Table 2. Energies for $[CB[5] + M']^+ + MX \rightarrow [CB[5] + MM'X]^+$ Computed at the M06-2X/6-31+G* Level of Theory

	energies for MX + $[CB[5] + M']^+ \rightarrow [CB[5] + MM'X]^+$ (kJ mol ⁻¹)							
MX	[Cl@CB[5] + NaK]+	[Cl@CB[5] + KRb]+	[Br@CB[5] + NaK]+	$[Br \cdot CB[5] + NaK]^+$				
NaCl	-374							
KCl	-418	-384						
RbCl		-362						
NaBr			-404	-206				
KBr			-455	-258				

containing complexes and a range of 28 kJ mol⁻¹ for those containing K.

The thermodynamic binding energies of the experimentally observed mixed metal halide complexes at 0 K were also calculated and compared. The results are shown in Table 2. For mixed NaK caps, loss of NaCl requires about 44 kJ mol⁻¹ less net energy than the loss of KCl. Loss of the corresponding bromides is 30-40 kJ mol⁻¹ higher in energy than chloride losses, and loss of NaBr requires 51 kJ mol⁻¹ less energy than the loss of KBr. For mixed KRb caps, loss of RbCl requires 22 kJ mol⁻¹ less energy than the loss of KCl. Loss of external bromides, from [Br·CB[5] + NaK]+, is easier than the loss of internally bound bromides, but again the loss of NaBr requires less energy (about 52 kJ mol⁻¹ less) than the loss of KBr. The thermodynamic calculations therefore predict that K⁺ will be preferentially retained on the CB[5] host when any of these complexes dissociate, as observed experimentally (Figures 5, S3 and 6).

SORI experiments should reflect the differences in energetic barriers to the dissociation of the complexes, and in the case of internally bound anions, they should reflect barriers to egress of the various anions from the central cavity of the CB[5] host molecule. We therefore carried out calculations to compare the barriers for MX (M = Na or K; X = F, Cl, Br, or I) loss from various $[X@CB[5]MM']^+$ complexes. The results of these calculations are plotted in Figure S5, and the computed barriers are compiled in Table 3. The computed barrier heights are strongly halogen-dependent, increasing in the order F < Cl

Table 3. Barriers for MX Loss from $[X@CB[5]MM']^+$ Computed at MMFF//M06-2X/6-31+G* Level of Theory, $kJ\ mol^{-1}$

X	NaX from XNa ₂	NaX from XNaK	KX from XNaK	KX from XK ₂	KX from XKRb	RbX from XKRb
F	265	250	308	321 ^a	ь	ь
Cl	373	355	397	381	363	385
Br	394	375	422	404	ь	ь
I	457	457	478	477	ь	ь

^aThis dissociation involved pulling K^+ through the CB[5] cavity along with the departing F^- , which is mechanistically different from all the others. ^bNot computed.

< Br < I, and less strongly dependent on which metal ions cap the complex. Barriers to NaX loss are consistently less than the barriers to KX loss. From the mixed metal complexes, NaX loss always occurs at lower energy than KX loss from the same complex, although the difference between these two dissociation channels decreases with increasing halide size. We also modeled the barriers to loss of KCl and RbCl from [Cl@CB[5] + KRb]+ for comparison with the experimentally observed dissociation of this ion. These calculations yielded a barrier of 363 kJ mol $^{-1}$ for KCl loss and of 385 kJ mol $^{-1}$ for RbCl loss. Whereas the thermodynamic calculations are consistent with the experimental observations (more facile loss of RbCl, Figure S3), these barrier calculations for the Rbcontaining complexes are not.

DISCUSSION

Structure and Size-Based Anion Selectivity in CB[5]-Metal Halide Complexes. Modeling suggests that anions may be bound on CB[5]-metal ion complexes either inside the CB[5] cavity between the two metal cations or outside the cavity, with the potential energy surface for the various external binding sites being relatively flat (the energies of the external structures shown in Figure 9b-d are all within 16 kJ mol⁻¹ of each other, and the geometric convergence of each of these structures was slow due to small changes in energy gradients with the halide position). Computational results (Table 1) show that the internally bound anion isomers are much lower in energy than the externally bound isomers, even for large anions such as iodide. Therefore, according to the calculations, the internal isomers are strongly favored thermodynamically, and any observed external isomers would have to be kinetically trapped, presumably because the barrier to entering the cavity is large. The barrier calculations summarized in Table 3 are consistent with this explanation, as they suggest that Cl- can pass through the CB[5] portal at energies 20-25 kJ mol⁻¹ less than that required for Br-, with I- requiring at least 40 kJ mol⁻¹ more than Br⁻.

X-ray data indicate that the portal of CB[5] has a radius of about 120 pm, whereas the internal cavity is larger, with a radius of about 220 pm.³⁴ Comparison with the sizes of the halide anions (Table 1) indicates that F⁻, Cl⁻, Br⁻, and I⁻ are all small enough to fit within the binding cavity but that all but

F⁻ are larger than the equilibrium size of the portal. Thus, simply based on size considerations, we might expect internal binding of the halides to be favorable thermodynamically, but that there could be significant kinetic barriers to passing through the portal and entering the internal cavity, with the barriers increasing with anion size, as Table 3 indicates is the case. Therefore, we believe that the size-selective halide binding observed in CB[5] complexes originates from differing abilities to pass through the CB[5] portal. We will now examine binding selectivity for each of the halides.

Fluoride Complexes. We attempted to spray CB[5] in the presence of fluoride salts, but no complexes containing F^- were observed, despite the fact that F^- should be small enough to enter the CB[5] cavity and to bind strongly there. Perhaps, the high solvation energy of F^- and its ability to act as a good hydrogen-bond acceptor prevented the formation or observation of any complexes under the conditions of our experiments, which involved electrospray from 50:50 isopropanol/water solvent, in which we expect that fluoride has a very high solvation energy.

Chloride Complexes. As noted earlier, inclusion of Cl⁻ within the central cavity of CB[5]—metal complexes has previously been demonstrated via single-crystal X-ray diffraction. ^{8,9} In the gas phase, ³⁶ we expect the internally bound anion structures to be similar to those characterized in the solid state, with the metal cations binding to the portal carbonyl oxygen atoms of the cucurbituril and with halide anions such as Cl⁻ bound inside the CB[5] cavity.

Our results for chloride complexes are consistent with these expectations. Chloride-containing complexes were easily observed. All dissociate at relatively high energies (Figure 4) and have CRAFTI cross sections similar to, or smaller than, those of [CB[5] + Na]⁺ (Figure 7). We might expect an internally bound Cl⁻ to cause overall contraction of the complex as the negative charge attracts the positive alkali metal cations and pulls them inward. Internal binding is consistent with the computational results (Table 1), which indicate that the internal binding of chloride is thermodynamically very favorable and that the energetic differences between the sodium- and potassium-capped complexes are small.

The results for the dissociation of [CB[5] + NaKCl]⁺ (Figure 5) are also consistent with the internal binding of Cl⁻. An internally bound structure could easily dissociate via either KCl or NaCl loss, and the thermodynamic energy differences obtained from the computational studies (Table 2) could qualitatively account for the observed 1:3 branching ratio between these two dissociation channels. The computed egress barriers for MCl losses from [CB[5] + NaKCl]⁺ (Table 3) differ by about the same amount as the binding energies and also favor the loss of NaCl, as observed. We believe that this is good evidence that chloride binds strongly within the CB[5] cavity in the gas phase, with only minor differences as the alkali metal cations are varied. Therefore, the CB[5] portal, nominally about 120 pm in radius, must be flexible enough at thermal energies to easily allow the passage of 167 pm Cl⁻.

Bromide Complexes. The results are different for larger halide guests such as Br⁻. Bromide is about 15 pm larger in radius than chloride, and the behavior of the bromide-containing complexes exhibits interesting complexity. The SORI results (Figure 4) suggest at least two isomers for the Br⁻ complexes containing Na⁺: one that is weakly bound, presumably with Br⁻ on the exterior of CB[5], and a more strongly bound isomer, presumably with Br⁻ inside the CB[5]

cavity. The multi-CRAFTI experiments (Figure 7) indicate that the cross sections of the observed [CB[5] + Na₂Br]⁺ complexes are smaller than that of [CB[5] + Na]⁺, consistent with the bromide bound inside the CB[5] cavity, drawing the two capping cations inward. This suggests that only the more strongly bound, internal isomers contribute to the multi-CRAFTI measurements. It is likely that the 60% portion of the population in which bromide is bound outside did not contribute to the cross-section measurements because it is so weakly bound (about 212 kJ mol⁻¹ according to the calculations shown in Table 1) that the external complexes dissociated (perhaps due to residual energy deposited in the process of desolvating and isolating the ions)³⁷ prior to the cross-section determination. Similarly, $[CB[5] + NaKBr]^+$ also gave cross sections comparable to or smaller than that of [CB[5] + Na]⁺ at all collision energies, again consistent with an internally bound complex and dissociative loss of the externally bound isomers prior to the cross section measure-

SORI measurements of the $[CB[5] + K_2Br]^+$ complex (Figure 4) detected only ions that dissociate at low energies, and the multi-CRAFTI results for this complex (Figure 7) are consistent with Br^- bound on the exterior of CB[5], as they indicate $[CB[5] + K_2Br]^+$ has a significantly greater CCS than $[CB[5] + Na]^+$ at all examined energies. These complexes have somewhat higher binding energies than those containing Na^+ capping cations (Tables 1 and 2) and apparently survive long enough for the cross-section measurement.

Overall, the data indicate that the CB[5] portal only allows Br⁻ entry when stretched significantly beyond its equilibrium size at thermal energies. Perhaps, heating the complexes would allow more Br⁻ ingress.

As for the structures of the externally bound bromide complexes, the SORI experiments on [CB[5] + NaKBr]+ (Figure 6) also shed some light. The complexes dissociating at very low energies yield both loss of NaBr and loss of KBr, with the NaBr loss products more abundant by a factor of about 4. This suggests that either there is one isomer with Br in approximately equal proximity to the two metal ions or there are two (or more) isomers with very similar energies that produce these two products. The computed lowest energy external structure, Figure 9b, is consistent with this expectation as the bromide ion lies on the equator of CB[5], approximately equidistant between the two capping cations such that this isomer might be expected to produce both NaBr and KBr products. The structures of Figure 9c,d are close to each other in energy and might also account for the observed products. The two structures in which Br is bound to only one metal ion (Figure 9f) and the corresponding structure with Brproximate to K⁺ (not shown) are calculated to be 81 and 97 kJ mol⁻¹ higher in energy, respectively, than the equatorially bound structure (Figure 9b). The two structures with both cations and the anion on the same CB[5] portal are at comparably higher energies. Thus, we favor the equatorial structure (Figure 9b) as the most consistent with the SORI experiment and the calculations.

lodide Complexes. At 206 pm radius, iodide is evidently too large to pass through the CB[5] portal at the energies of these experiments as no iodide-containing complexes of CB[5] with singly charged alkali cation caps were observed. The failure to observe externally bound iodide is interesting in that the calculated stabilities of the externally bound iodide complexes are only slightly less than those of the externally

bound bromides (Table 1), which were observed. This may reflect a weakness in using the M06-2X functional with modest basis sets to compute energies for complexes that include highly polarizable anions such as I-; more dispersion correction may be needed than that this approach provides. In any event, the CB[5] portal appears to be exquisitely sensitive to the size of potential anionic guests.

The observation of externally bound bromide complexes with specific metal caps encouraged us to try more highly charged metals (+2 alkaline earth cations) to see if the higher charge might stabilize externally bound I complexes. [CB[5] + SrI]⁺, [CB[5] + NaSrI]²⁺, [CB[5] + BaI]⁺, and [CB[5] + NaBaI]2+ were all observed, whereas no triply charged complexes composed of two alkaline earth metals and a halide were detected (Figures 3 and S2). Based on the multi-CRAFTI results (Figures 8 and S4), all of these complexes bind the iodide externally, as expected, given the large size of this anion and the corresponding high barrier to passage into the CB[5] interior. The observation of [CB[5] + SrI]+, [CB[5] + NaSrI]²⁺, [CB[5] + BaI]⁺, and [CB[5] + NaBaI]²⁺ supports the idea that more highly charged cations are more efficient polarizers with a greater ability to stabilize the guest-host systems and bind even large anions, albeit on the exterior of the CB[5] host.

Influence of Capping Cations on Internal versus **External Binding.** The data suggest the capping metal ions influence the preference for internal versus external binding. The SORI results (Figure 4) indicate that under the conditions of our experiments, the observed [CB[5] + Na₂Br]⁺ was 60% weakly bound (external) and 40% strongly bound (internal), that [CB[5] + NaKBr]+ was 90% external and 10% internal, and that $[CB[5] + K_2Br]^+$ was essentially 100% external. This is reasonably consistent with the computational results for binding strengths (Table 1) and egress barriers (Table 3); external binding is 36 kJ mol⁻¹ stronger for K⁺ than for Na⁺ (Table 1), and the barrier for MBr loss (and for Br ingress) is 10 kJ mol⁻¹ greater for two K⁺ capping cations than for two Na⁺ capping cations (Table 3). It is possible that this increase in barrier energy results from placing the larger K⁺ on one portal, forcing the other portal to tighten up somewhat. Similarly, the dissociation of [CB[5] + NaKBr]+, which, as noted above, is probably mostly an externally bound bromide structure, resulted in 75% loss of NaBr and 25% loss of KBr (Figure 6) because KBr loss requires greater energy. Overall, the substitution of Na+ by K+ in these complexes leads to increased preference for the external binding of Br-. This dependence of anion binding site selectivity on metal ion probably deserves further investigation.

CONCLUSIONS

This work demonstrates that cucurbit[n]uril—metal complexes can be size-selective anion receptors and that this can be observed using mass spectrometric methods. In fact, cucurbit[5]uril is probably better described in the present context as an ion-pair receptor, as cations bind on the portal of the host and anions, in close contact with the cations, bind selectively in the cucurbituril interior and nonselectively outside the host. We found that Cl binds inside CB[5] complexed with various alkali metals; Br binds both inside (with Na⁺-capped CB[5] portals) and outside the CB[5] cavity (when K⁺ is the capping cation). I⁻ complexes were not observed with alkali metal cations serving as caps, but I does bind strongly enough to the exterior in the presence of alkaline

earth cation caps to be observed in electrospray mass spectrometry. Finally, the results obtained from multi-CRAFTI are consistent with the dissociation behavior observed from SORI-CID experiments and with computational calculations. This increases our confidence in the multi-CRAFTI method.

ASSOCIATED CONTENT

Supporting Information

The Supporting Information is available free of charge at https://pubs.acs.org/doi/10.1021/acs.jpca.1c05060.

Electrospray mass spectrum for CB[5] mixed with NaBr and KBr; electrospray mass spectrum for CB[5] mixed with BaI2; SORI data for the dissociation of [CB[5] + KRbCl]+; multi-CRAFTI results for [CB[5] + NaBaI]²⁺ versus [CB[5] + Ba]²⁺; and computed potential energy profiles for the loss of MX from $[X@CB[5]MM']^+$ (M =Na, K; X = F, Cl, Br, I) (PDF)

AUTHOR INFORMATION

Corresponding Author

David V. Dearden - Department of Chemistry and Biochemistry, Brigham Young University, Provo, Utah 84602, United States; orcid.org/0000-0003-0899-7776; Email: dvd@chem.byu.edu

Authors

Tina Heravi – Department of Chemistry and Biochemistry, Brigham Young University, Provo, Utah 84602, United

Jiewen Shen – Department of Chemistry and Biochemistry, Brigham Young University, Provo, Utah 84602, United States

Spencer Johnson - Department of Chemistry and Biochemistry, Brigham Young University, Provo, Utah 84602, United States

Matthew C. Asplund - Department of Chemistry and Biochemistry, Brigham Young University, Provo, Utah 84602, United States

Complete contact information is available at: https://pubs.acs.org/10.1021/acs.jpca.1c05060

Author Contributions

T.H. and J.S.contributed equally.

The authors declare no competing financial interest.

ACKNOWLEDGMENTS

We are grateful to the U. S. National Science Foundation for support of this work (CHE-1904838), to the BYU College of Physical and Mathematical Sciences for funds to support undergraduate research, and to the BYU Office of Research Computing for computational resources.

REFERENCES

(1) Chen, L.; Berry, S. N.; Wu, X.; Howe, E. N. W.; Gale, P. A. Advances in anion receptor chemistry. Chem 2020, 6, 61-141. (2) Li, Y.; Flood, A. H. Strong, size-selective, and electronically tunable C-H • • • halide binding with steric control over aggregation from synthetically modular, shape-persistent [3₄]triazolophanes. J. Am. Chem. Soc. 2008, 130, 12111-12122.

- (3) Davis, J. T.; Gale, P. A.; Quesada, R. Advances in anion transport and supramolecular medicinal chemistry. *Chem. Soc. Rev.* **2020**, *49*, 6056–6086.
- (4) Wu, X.; Gilchrist, A. M.; Gale, P. A. Prospects and challenges in anion recognition and transport. *Chem* **2020**, *6*, 1296–1309.
- (5) Isaacs, L. Cucurbit[n]urils: From mechanism to structure and function. *Chem. Commun.* **2009**, 619–629.
- (6) Masson, E.; Ling, X.; Joseph, R.; Kyeremeh-Mensah, L.; Lu, X. Cucurbituril chemistry: A tale of supramolecular success. *RSC Adv.* **2012**, *2*, 1213–1247.
- (7) Shen, J.; Dearden, D. V. Recent progress in gas phase cucurbit nuril chemistry. *Isr. J. Chem.* **2018**, *58*, 225–229.
- (8) Liu, J.-X.; Long, L.-S.; Huang, R.-B.; Zheng, L.-S. Interesting anion-inclusion behavior of cucurbit[5]uril and its lanthanide-capped molecular capsule. *Inorg. Chem.* **2007**, *46*, 10168–10173.
- (9) Liu, J.-X.; Long, L.-S.; Huang, R.-B.; Zheng, L.-S. Molecular capsules based on cucurbit[5]uril encapsulating "naked" anion chlorine. *Cryst. Growth Des.* **2006**, *6*, 2611–2614.
- (10) Zhang, Y.-Q.; Zhu, Q.-J.; Xue, S.-F.; Tao, Z. Chlorine anion encapsulation by molecular capsules based on cucurbit[5]uril and decamethylcucurbit[5]uril. *Molecules* **2007**, *12*, 1325–1333.
- (11) Fiala, T.; Sleziakova, K.; Marsalek, K.; Salvadori, K.; Sindelar, V. Thermodynamics of halide binding to a neutral bambusuril in water and organic solvents. *J. Org. Chem.* **2018**, *83*, 1903–1912.
- (12) Havel, V.; Babiak, M.; Sindelar, V. Modulation of bambusuril anion affinity in water. *Chem.–Eur. J.* **2017**, *23*, 8963–8968.
- (13) Révész, Á.; Schröder, D.; Svec, J.; Wimmerová, M.; Sindelar, V. Anion binding by bambus[6]uril probed in the gas phase and in solution. *J. Phys. Chem. A* **2011**, *115*, 11378–11386.
- (14) Öeren, M.; Shmatova, E.; Tamm, T.; Aav, R. Computational and ion mobility MS study of (all-s)-cyclohexylhemicucurbit[6]uril structure and complexes. *Phys. Chem. Chem. Phys.* **2014**, *16*, 19198–19205.
- (15) Gauthier, J. W.; Trautman, T. R.; Jacobson, D. B. Sustained off-resonance irradiation for collision-activated dissociation involving Fourier-transform mass-spectrometry collision-activated dissociation technique that emulates infrared multiphoton dissociation. *Anal. Chim. Acta* 1991, 246, 211–225.
- (16) Guan, S.; Marshall, A. G.; Wahl, M. C. MS/MS with high detection efficiency and mass resolving power for product ions in Fourier transform ion cyclotron resonance mass spectrometry. *Anal. Chem.* 1994, 66, 1363–1367.
- (17) Yang, F.; Voelkel, J. E.; Dearden, D. V. Collision cross sectional areas from analysis of Fourier transform ion cyclotron resonance line width: A new method for characterizing molecular structure. *Anal. Chem.* **2012**, *84*, 4851–4857.
- (18) Yang, F.; Jones, C. A.; Dearden, D. V. Effects of kinetic energy and collision gas on measurement of cross sections by Fourier transform ion cyclotron resonance mass spectrometry. *Int. J. Mass Spectrom.* **2015**, *378*, 143–150.
- (19) Anupriya; Jones, C. A.; Dearden, D. V. Collision cross sections for 20 protonated amino acids: Fourier transform ion cyclotron resonance and ion mobility results. *J. Am. Soc. Mass Spectrom.* **2016**, 27, 1366–1375.
- (20) Anupriya; Gustafson, E.; Mortensen, D. N.; Dearden, D. V. Quantitative collision cross-sections from FTICR linewidth measurments: Improvements in theory and experiment. *J. Am. Soc. Mass Spectrom.* **2018**, *29*, 251–259.
- (21) Sievers, H. L.; Grützmacher, H.-F.; Caravatti, P. The geometrical factor of infinitely long cylindrical ICR cells for collision energy-resolved mass spectrometry: Appearance energies of EI₂⁺ (E=P, As, Sb, and Bi) from collision-induced dissociation of EI₃⁺ and [EI•ligand]⁺ complexes. *Int. J. Mass Spectrom. Ion Processes* **1996**, 157−158, 233−247.
- (22) Blakney, G. T.; Hendrickson, C. L.; Marshall, A. G. Predator data station: A fast data acquisition system for advanced FT-ICR MS experiments. *Int. J. Mass Spectrom.* **2011**, *306*, 246–252.

- (23) Jiao, C. Q.; Ranatunga, D. R. A.; Vaughn, W. E.; Freiser, B. S. A pulsed-leak valve for use with ion trapping mass spectrometers. *J. Am. Soc. Mass Spectrom.* **1996**, *7*, 118–122.
- (24) Wigger, M.; Nawrocki, J. P.; Watson, C. H.; Eyler, J. R.; Benner, S. A. Assessing enzyme-substrate specificity using combinatorial libraries and electrospray ionization-Fourier transform ion cyclotron resonance mass spectrometry. *Rapid Commun. Mass Spectrom.* **1997**, *11*, 1749–1752.
- (25) Guan, S.; Marshall, A. G. Stored waveform inverse Fourier transform (SWIFT) ion excitation in trapped-ion mass spectometry: Theory and applications. *Int. J. Mass Spectrom. Ion Processes* **1996**, 157–158, 5–37.
- (26) Laskin, J.; Futrell, J. H. Activation of large ions in FT-ICR mass spectrometry. *Mass Spectrom. Rev.* **2005**, 24, 135–167.
- (27) Zhang, H.; Ferrell, T. A.; Asplund, M. C.; Dearden, D. V. Molecular beads on a charged molecular string: α,ω-alkyldiammonium complexes of cucurbit[6]uril in the gas phase. *Int. J. Mass Spectrom.* **2007**, 265, 187–196.
- (28) Valiev, M.; Bylaska, E. J.; Govind, N.; Kowalski, K.; Straatsma, T. P.; Van Dam, H. J. J.; Wang, D.; Nieplocha, J.; Apra, E.; Windus, T. L.; et al. NWChem: A comprehensive and scalable open-source solution for large scale molecular simulations. *Comput. Phys. Commun.* **2010**, *181*, 1477–1489.
- (29) Kebarle, P. A brief overview of the present status of the mechanisms involved in electrospray mass spectrometry. *J. Mass Spectrom.* **2000**, 35, 804–817.
- (30) Benkestock, K.; Sundqvist, G.; Edlund, P. O.; Roeraade, J. Influence of droplet size, capillary-cone distance and selected instrumental parameters for the analysis of noncovalent protein-ligand complexes by nano-electrospray ionization mass spectrometry. *J. Mass Spectrom.* **2004**, *39*, 1059–1067.
- (31) Metwally, H.; McAllister, R. G.; Konermann, L. Exploring the mechanism of salt-induced signal suppression in protein electrospray mass spectrometry using experiments and molecular dynamics simulations. *Anal. Chem.* **2015**, *87*, 2434–2442.
- (32) Schröder, D. Applications of electrospray ionization mass spectrometry in mechanistic studies and catalysis research. *Acc. Chem. Res.* **2012**, *45*, 1521–1532.
- (33) Shannon, R. D. Revised effective ionic radii and systematic studies of interatomic distances in halides and chalcogenides. *Acta Crystallogr., Sect. A: Found. Crystallogr.* **1976**, 32, 751–767.
- (34) Lee, J. W.; Samal, S.; Selvapalam, N.; Kim, H.-J.; Kim, K. Cucurbituril homologues and derivatives: New opportunities in supramolecular chemistry. *Acc. Chem. Res.* **2003**, *36*, 621–630.
- (35) Shannon, R. D. Revised effective ionic-radii and systematic studies of interatomic distances in halides and chalcogenides. *Acta Crystallogr., Sect. A: Cryst. Phys., Diffr., Theor. Gen. Crystallogr.* **1976**, 32, 751–767.
- (36) Kellersberger, K. A.; Anderson, J. D.; Ward, S. M.; Krakowiak, K. E.; Dearden, D. V. Encapsulation of N_2 , O_2 , methanol, or acetonitrile by decamethylcucurbit[S]uril(NH_4^+)₂ complexes in the gas phase: Influence of the guest on 'lid' tightness. *J. Am. Chem. Soc.* **2001**, *123*, 11316–11317.
- (37) Mortensen, D. N.; Jones, C. A.; Dearden, D. V. Appropriate choice of event length in sustained off-resonance irradiation collision-induced dissociation (SORI-CID) experiments: Activated ion collision-induced dissociation. *Int. J. Mass Spectrom.* **2012**, 330–332, 241–245.